Nafion membranes reinforced by cellulose nanocrystals for fuel cell applications: aspect ratio and heat treatment effects on physical properties

Arayik Hambardzumyan, Marylène Vayer, Laurence Foulon, Miguel Pernes, Thierry Devers, Janick Bigarré, Véronique Aguié-Béghin

Nafion membranes reinforced by cellulose nanocrystals for fuel cell applications: aspect ratio and heat treatment effects on physical properties

Arayik Hambardzumyan[1,2], Marylène Vayer[1], Laurence Foulon[3], Miguel Pernes[3], Thierry Devers[2], Janick Bigarré[4] ,Véronique Aguié-Béghin[3,*]

[1]Interfaces, Confinement, Matériaux et Nanostructures (ICMN), CNRS-Université d'Orléans, UMR 7374, 1b, Rue de la Férollerie, C.S. 40059, 45071 Orléans Cedex 2, France
[2]Interfaces, Confinement, Matériaux et Nanostructures (ICMN), CNRS-Université d'Orléans, site de Chartres, 21 rue de Loigny la Bataille, 28000, Chartres, France
[3] Université de Reims Champagne Ardenne, INRAE, FARE, UMR A 614, 51097 Reims, France
[4]CEA, DAM, Le Ripault, BP16, F-37260 Monts, France

*Corresponding Author
Preprint published in J. Mater. Sci. : https://doi.org/10.1007/s10853-022-06921-6

Abstract

This study explored the improvement of the physicochemical properties (mechanical resistance, water uptake, swelling…) of Nafion membranes by cellulose nanocrystals (CNCs). These composite membranes were prepared from Ramie and Tunicate nanocrystals with respective aspect ratios of about 28 and 106. It was demonstrated that, regardless of the type of nanocrystals, increasing the cellulose weight content from 0 to 10 wt. % increased the water uptake and the thickness swelling, and decreased the in-plane swelling of the composite membranes during water immersion. The mechanical performances of the composite membranes (tensile strength, elongation at break and Young modulus) were also enhanced, with the best compromise for Tunicate nanocrystals found to be 5 wt. %. The effect of thermal annealing up to 150°C on the Nafion-Tunicate 5 wt. % composite was tested and compared to that of pure Nafion. With thermal annealing, a small decrease in water uptake capacity, protonic conductivity, ion exchange capacity and hydration number was observed for both membranes. At the sub-molecular level, FTIR data suggest that the heat treatment of Nafion-Tunicate membranes induces cross-linking reactions between sulfonic groups of Nafion chains and surface functional groups of CNCs, leading for example to sulfonic ester links. The exothermic peak observed by DSC can assigned an increase of the crystalline phase of Nafion chains and especially in the vicinity of CNCs. All cross-linkages led to an improvement in the mechanical resistance of the membranes when thermal annealing was below 130°C.

Graphical abstract

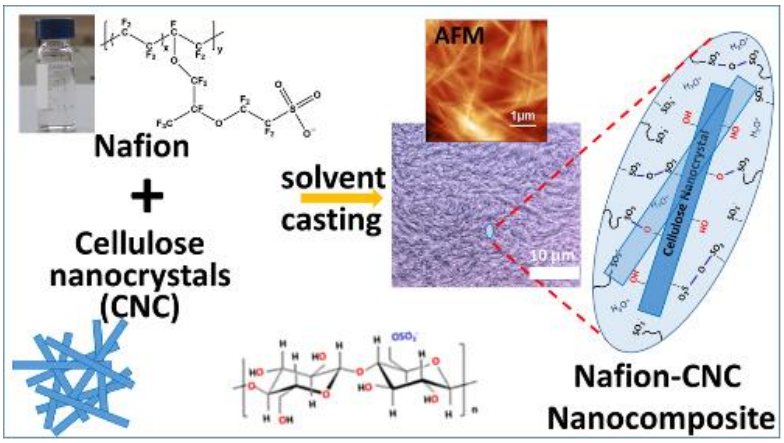

Keywords

Nafion, cellulose nanocrystals, Proton exchange membrane fuel cell, composite,

Introduction

The proton exchange membrane fuel cell (PEMFC) technology is one of the most promising alternative ways to convert chemical energy to electrical energy [1-5]. Among the polymer membranes developed [6], one of the most widely used is composed of perfluorosulfonic acid polymers (PFSA) such as Nafion [1, 7-10]. Its proton conductivity is in the range of 1 to 21.5 S m^{-1} and depends on the water content [11]. The cost, high methanol permeability and low proton conductivity at temperatures above 80°C are the main factors that limit its application [12]. In order to find solutions to guarantee high local mobilities of the proton solvent and the protonic charge carriers in the polymer matrix even at high temperature [11], and to improve the physical and mechanical properties, it is necessary to replace low-temperature Nafion-based PEMFCs (working at 60-80°C) by higher-temperature PEMFCs with operating temperatures between 100 and 200°C, using an appropriate water management system. This would increase the lifetime of fuel cells but remains a major challenge [6, 10, 13-18].

In recent years, the enhancement of the mechanical properties of Nafion has been the subject of numerous empirical and theoretical studies [15-17]. Several preparations of Nafion-composite membranes combining either organic or inorganic fillers with Nafion have been investigated. Among the large number of fillers tested, the incorporation of 0.5-20 wt. % hydrophilic inorganic oxides such as SiO_2 [3, 9, 19-23],TiO_2 [24] and ZrO_2 [25] has been proposed to improve water uptake and the thermomechanical stability of the membranes but also to improve proton conductivity. Other fillers use functionalized clays [26], functionalized graphene oxide [27], sulfonated carbon-nanotubes [28], dopants derived from phosphonic acid [29] generating additional proton-conducting sites and increasing water uptake and retention capacity of nanohybrid membranes.

Organic polymers such as polytetra-fluoroethylene [30, 31], polyben-zimidazole

[32], poly (vinyl alcohol) [33], polypyrrole [34], sulfonated covalent organic nanosheets [35] or sulfonated poly(arylene ether ketone) [36] have also been added to Nafion with the aim of improving proton conductivity, dimensional stability and water uptake.

In the last two decades, nanocelluloses have proved to be very worthwhile and are now used in composites for advanced functional applications [37-43]. Compared to inorganic or other polymeric materials, nanocelluloses have attracted interest thanks to their potential to replace petroleum-based composites, thereby contributing to sustainable economic development [3, 44]. Among nanocellulose materials, cellulose nanocrystals (CNCs) are rigid rod-shaped crystalline particles with a high aspect ratio (from 20 to 100) depending on their origin, either from lignocellulosic fibers or from the tunic of mollusks, e.g. Tunicate [43]. They are usually isolated by mild controlled hydrolysis using sulfuric acid, in which the crystalline regions of the cellulose fibers are separated from the hydrolyzed amorphous zones. CNC rods contain hydrophilic faces with hydroxyl groups and hydrophobic ones [45]. They enhance the mechanical properties of the composites in which they are incorporated due to their capacity to form a rigid network resulting from strong hydrogen-bonding interactions between adjacent nanocrystals and/or between the nanocrystals and the hydrophilic polymer matrix [37, 39]. More recently, it has been shown that cellulose nanocrystals or nanofibrils may be a promising sustainable and environmentally beneficial nanomaterial for green and renewable electronics, and for energy applications such as solar cells, piezoelectric materials or electroconductive materials [46-48] but also for fuel cell applications [12, 49]. The inclusion of CNC in Nafion membranes without thermal treatment enhanced the proton conductivity and suppressed the methanol permeability [50]. Jiang et al. [51] prepared Nafion based membranes with bacterial cellulose and observed the positive effect of an annealing treatment at 110°C for 1h with a maximum performance of PEMFC membranes of 100 mW. cm^{-2} (compared to 60 $mW.cm^{-2}$ for pure Nafion). Noonan et al. [47] produced hybrid cellulose membranes by mixing Nafion with cellulose nanofibrils extracted from Kraft softwood pulp to reduce the cost and enhance the mechanical and thermal properties of Nafion membranes.

In view of all these bioeconomic challenges, this work offers a new design for Nafion-based membranes by adding two types of CNC preparations, differentiated by their origin, aspect ratio and CNC content, and annealed at different temperatures. The objective was to exploit their promising potential in fuel cell membranes by improving essential properties such as dimensional stability in a humid environment, mechanical properties, and ion exchange capacity (IEC) and protonic conductivity. These measurements were completed by structural analysis through a combination of spectrophotometric (or spectroscopic), topographic and physico-chemical water sorption methods in order to assess functional groups and the level of interaction between the cellulose and the Nafion polymer. They were completed by measurement of their thermal properties. This multiple approach showed that Nafion-CNC membranes can meet a number of essential criteria for PEMFC applications such as the improvement of mechanical properties while maintaining their dimensional stability, ion exchange capacity and proton conductivity during swelling, up to a limited CNC content and for high aspect ratio of CNC.

Materials and methods

Materials

A solution of Nafion 2020 in isopropanol was purchased from DuPont (US). Sulfuric acid 98% and dimethyl sulfoxide (DMSO) ≥ 99.5% were purchased from Roth Sochiel (France). De-ionized water with a resistivity of 0.055 Ω^{-1} cm^{-1} was used throughout the study.

CNC preparation

Ramie and Tunicate nanocrystals were prepared by sulfuric acid hydrolysis from Ramie fibers (*Boehmeria nivea*) and the tunic of *Microscosmus fulcatus* respectively as described before [43, 52]. Small pieces of Ramie fibers were cut and treated with 2% NaOH at 20 °C for 48 h in order to remove any hemicelluloses, traces of pectin or residual proteins. In parallel, small fragments of the external wall of the Tunicates were treated three times with a solution of KOH (5%, w/v), washed, submitted to four successive bleaching treatments and finally disintegrated in water with a Waring blender. The homogeneous suspensions obtained from washed Ramie fibers and Tunicate were submitted to overnight hydrolysis (∼16 h) with 65% (w/w) H_2SO_4 at 35 °C under stirring. During the acidic treatment, amorphous cellulosic regions are hydrolyzed, leading to nanoparticles charged by ester sulfate groups (HSO_3^-). The resulting suspensions were centrifuge washed with water until neutral pH and dialyzed using a 6000 molecular weight cutoff regenerated cellulose membrane. The sulfate ester groups link to cellulose nanocrystal surface (0.4-0.5 charge nm^{-2}) allow to obtain stable colloidal CNC suspension in water [42]. It was stored at 4°C and sonicated for several minutes using a Sonics vibra-cell (750W, Fisher-Bioblock) at an appropriate concentration before use. The average crystal lengths, sections and aspect ratios were evaluated from analysis of AFM profile images (Fig. SI-1 and previous data [53]). The sulfur content was estimated from elementary microanalysis (ISA, CNRS, Lyon). These results as well as their mechanical properties and crystalline form are summarized in Table 1.

Table 1. Physico-chemical characteristics of isolated Ramie (R) and Tunicate (T) nanocrystals

CNC	Length (nm)	d (nm)	L/d	Young Modulus (GPa) longitudinal[a]	crystalline form[b]	Sulfur[c] (wt. %)
R	180.9±12.5	6.3±0.4	28.7±4.1	120-138	Iβ/Iα	0.8 ± 0.2
T	1056.0 ± 28.5	10.0 ± 0.5	105.6±8.5	150.7 ±28.8	Iβ	0.7 ± 0.2

[a] from [54, 55] [b][56] [c] as in [42]

Preparation of Nafion-Ramie (N-R) and Nafion-Tunicate (N-T) membranes

Nafion based membranes were prepared from Nafion solution (22.3 wt. %) in isopropanol and from Ramie (2.3 wt. %) or Tunicate (1.1 wt. %) CNC aqueous suspensions. First, isopropanol

and water were exchanged with DMSO. Ramie and Tunicate CNC aqueous suspensions were dispersed in water-DMSO (50/50) solvent before evaporating any remaining traces of water by stirring (500 rpm) in a water-bath at ~100°C during 2 hours. Because of the marked difference in the boiling points of water and DMSO (100 and 189°C, respectively) CNC suspensions in DMSO with a residual water content estimated at less than 4 % were obtained. In the second step, each CNC suspension in DMSO was mixed with Nafion polymer solution in DMSO and stirred for 2 hours (500 rpm) at ambient temperature to obtain homogeneous and stable colloidal mixtures with a final CNC content ranging from 0 to 10 wt. % (see SI-2).

Nafion-CNC membranes were prepared using a Film Applicator (Model KCC 202 from ERICHSEN GmbH, Hemer, DE) composed of a heated glass plate (adjustable temperature varying from ambient to 200°C) and micrometric applicator, which at room temperature spreads the mixture on the glass plate at the chosen forward speed of 2 m. min^{-1} and with a blade height at 500 µm. The "wet membrane" was then left on the plate and heated at 100°C for 40 min to ensure the removal of DMSO and traces of water. Once cooled down, the membrane was carefully removed from the glass plate and stored at room temperature. All the Nafion-Ramie (N-R) and Nafion-Tunicate (N-T) composite membranes obtained in these conditions had an average thickness of 70 µm ± 10 µm estimated in ambient conditions from digital optical microscopy observations of each membrane section (SI-3).

Annealing treatment

A heat treatment in an oven was then applied, at 100°C during 5 min for the membranes named "*raw*" and then at higher temperatures, from 100 to 150°C during 1 hour for "*annealed*" membranes. It has been performed under atmospheric conditions.

Digital Optical Microscopy (DOM)

The morphology of the Nafion-CNC composite membranes was examined with a Keyence VHX-5000 digital optical microscope (DOM). General observation of the membranes was carried out at magnifications from x500 up to x5000.

Atomic Force Microscopy (AFM)

In order to characterize the surface morphology of the membranes, atomic force microscopy (AFM) in tapping mode was carried out in air with an ICON apparatus from Bruker. Silicon Tap 300 cantilevers from Budget Sensors with integrated symmetrical pyramidal tips (15 µm high) with no Al coating backside, a nominal spring constant of 42 $N \cdot m^{-1}$, and a resonance frequency of 300 kHz were used. A digital resolution of 512 × 512 pixels and a scanning rate of 1 Hz were used. For each condition, three images were acquired at different places on the membrane.

Scanning Electron Spectroscopy (SEM)

Each composite membrane was observed by scanning electron microscope (SEM, Zeiss Evo50 equipped with an Oxford energy dispersive X-ray detector). Samples were prepared by fracturing (freeze-casting in liquid N_2) small pieces of the membranes in order to make the internal part of the specimen accessible. A low energy was used (5 keV) in order to obtain the highest possible surface resolution. Before imaging, all the specimens were coated with approximately 20 nm of gold using a VCR high resolution indirect ion-beam sputtering system in order to prevent surface charging during the measurements.

Fourier Transform Infrared Spectroscopy (FTIR)

Fourier transform infrared (FTIR) spectra were recorded on coated films using a Nicolet 6700 spectrophotometer (Thermo Fisher Scientific, USA) by attenuated total reflectance (ATR). The measurements were performed in three replicates on each face of the membrane section (2 cm X 2 cm). The averaged spectra were obtained over a spectral range of 4000 to 400 cm^{-1} through 16 scans of the sample at a resolution of 4 cm^{-1} and corrected by baseline subtraction and unit vector normalization to a range of 4000 to 400 cm^{-1}.

Hygroscopic properties by dynamic vapor sorption (DVS)

A gravimetric sorption analyser (IGA, Intelligent Gravimetric Analyser, Hiden Isochema Ltd.) was used to determine the water sorption isotherm as described previously [55]. The experiment was performed at 20°C and the relative humidity (RH) values ranged from 5 to 95%. The membrane portions (5 mg) were hydrated in steps of RH during the water sorption and desorption phases. The sample mass was recorded throughout the process until equilibrium was reached. The water content (C) was calculated using Eq. (1), where m_{eq} is the mass of the sample in the equilibrium state and m_d is the mass of the dry sample measured after a drying sequence.

$$C = \frac{m_{eq} - m_d}{m_d} \quad (1)$$

This drying sequence consisted of a heating step at 40°C under a dry flow of nitrogen for 240 min. followed by a cooling step at 20°C under a dry flow of nitrogen for 480 min.

Water uptake and dimensional stability

Nafion-CNC membranes measuring 40 x 40 mm with different amounts of CNCs were carefully cut. They were first dried at 60°C for 1 night in order to remove trace of water. Then, the weights (W_{dry}), lengths (L_{dry}) and thicknesses (T_{dry}) of each membrane were measured. After soaking at room temperature in deionized water for 72 hours, the samples were removed from the water and the excess water was carefully adsorbed by filter paper. Their weights (W_{wet}), lengths (L_{wet}) and thicknesses (T_{wet}) were measured again at 25°C.

The water uptake (WU), in-plane swelling ratio (LS) and thickness swelling ratio (TS) of the membranes were calculated [18, 19, 35] using equations (2), (3) and (4).

$$WU = \frac{W_{wet} - W_{dry}}{W_{dry}} \quad (2)$$

$$LS = \frac{L_{wet} - L_{dry}}{L_{dry}} \quad (3)$$

$$TS = \frac{(T_{wet} - T_{dry})}{T_{dry}} \quad (4)$$

Lengths were measured by using a ruler with a resolution of 1 mm. Water uptake and swelling ratios were measured three times and average values were recorded. The relative errors on water up-take and swelling ratios were estimated at 5%. Thickness measurements were realized from Digital Optical Microscopic images of membranes taken before and after water uptake.

Ion exchange capacity (IEC) and hydration number (λ) of membranes

The ion exchange capacity (IEC) of the membranes was determined via acid-base titration. For this purpose, all the membranes were oven-dried at 60°C overnight. The membranes were then weighed (W_{dry}) before being immersed in a 2M NaCl solution for 24 h in order to completely release the protons. The liquid was titrated with 0.005M NaOH (C_{NaOH})

solution by pH meter. The experiment was repeated three times and IEC was calculated using Eq. (5), where V_{NaOH} is the volume of NaOH solution consumed.

$$IEC = \frac{V_{NaOH} * C_{NaOH}}{W_{dry}} \quad (5)$$

The hydration number of the membranes (λ) was calculated using Eq. (6), where WU is the water uptake and M_{H2O} is the molecular weight of water [36].

$$\lambda = \frac{n_{H_2O}}{n_{SO_3H}} = \frac{WU}{M_{H_2O} * IEC} \quad (6)$$

Mechanical properties tests

Stress-strain experiments were performed on Nafion-CNC samples using a LLOYD Instruments LF plus with a force sensor at 1 kN. Rectangular samples of 30 mm in length and 10 mm in width were cut from the membrane and then placed on a 1 kN dual lead screw tensile testing stage equipped with a 50 N load cell. The sample thickness was measured from the section film observed by Digital Optical Microscopy (SI-3). The initial length of the sample between the clamps was 20 mm. The analysis was performed at a speed of 5 $mm.min^{-1}$ until membrane rupture. The displacement and the force were recorded during the test, and the Young modulus, the fracture strain and tensile strength at break were then measured taking into account their respective dimensions in the calculation.

Thermogravimetric (TGA) and differential scanning calorimetry (DSC) analysis

The thermal properties of the membranes were determined by thermogravimetric and differential scanning calorimetry measurements using a TA Instruments Discovery SDT 650 and Discovery DSC 25 respectively. For TGA analysis, the heating rate was fixed at 10°C min^{-1} from 30°C until 800°C under nitrogen atmosphere using a flux of 100 mL min^{-1}. For DSC measurements, the heating rate was fixed at 10°C min^{-1} and two runs (from -50°C to 250°C for the first and from -50°C to 300°C for the second one) were performed under nitrogen atmosphere using a flux of 50 mL min^{-1}. For both the sample weight was about 11 mg.

Proton conductivity

The proton conductivity was measured using an impedance spectroscopy device equipped with a 4-electrode FUMATECH Cell. The sample was placed in water during 72h at room temperature in order to completely swell the membrane. After swelling, the sample was carefully cut with a scalpel to dimensions of 5mm x 40 mm and the thickness was measured with a Digimatic Absolute Mitutoyo 547-401 thickness gauge with a resolution of 1 µm. The sample was then placed on the electrodes. The impedance measurements were carried out using a SI 1260 spectrometer verified and calibrated once a year. The repeatability, measured on Nafion NRE112 with 10 samples, was greater than 95%. The membrane resistance R was measured by plotting real (Z') versus imaginary (Z'') parts in a Nyquist plot.
The proton conductivity was finally calculated by using Eq. (7), where L (in cm) is the inter-electrode distance, R (in kOhm) is the membrane resistance derived from the real axis intersect at high frequencies, and l (in cm) and t (cm) are the width and thickness of the sample, respectively.

$$\sigma\ (mS/cm) = \frac{L}{R * l * t} \quad (7)$$

The relative error on the proton conductivity measurement was estimated to be less than 10%.

Results and discussion

Structure and properties of Nafion-CNC raw membranes: Influence of the origin and CNC content.

Nafion-CNC based membranes were prepared with two distinct cellulose nanomaterials isolated by mild hydrolysis: one from plant fibers (Ramie, Boehmeria nivea), the second one from animal tunic (Tunicate, Microscosmus fulcatus). The Ramie and Tunicate nanocrystals are distinguished by their length, aspect ratio and crystalline form (Table 1 and Fig. SI-1). Both are made of highly crystalline cellulose I with high Young modulus values (longitudinal [56]). The influence of the origin (Ramie versus Tunicate) and CNC content (from 2.5 to 10 wt. %) was evaluated on the morphology of the membranes first and then on their swelling and mechanical properties. CNC distribution in raw membranes

CNC distribution in raw membranes

After a visual examination, microscopic observations were performed at different scales by DOM, SEM and AFM to evaluate the CNC distribution in the raw membranes annealed at 100°C for 5 min. All the membranes were colorless and transparent. Neither CNC aggregation nor phase separation was observed on the membrane surfaces, regardless of the origin and the CNC content (from 2.5 to 10 wt. %). As an example, Fig. 1 shows photographs, SEM and AFM topographic images of Nafion, Nafion-Ramie 5 wt. % (N-R 5 wt. %) and Nafion-Tunicate 5 wt. % (N-T 5 wt. %) raw membranes demonstrating a very good distribution of CNCs in the Nafion matrix. SEM and AFM images recorded on the surface or on the cross-sectional cut of the membranes displayed very good agreement of the structural shape differences between Ramie and Tunicate CNCs. Needle forms were clearly preserved according to their respective aspect ratio (Table 1 and Fig. SI-1). Fig SI-2 displays the images recorded by DOM for all the studied membranes. Moreover, after multiple washing in deionized water, no change in surface topography was observed, suggesting that the interaction between CNCs and Nafion was strong enough not to release CNC by water washings. This good affinity between the Nafion polyelectrolyte matrix and the CNCs without phase separation was already observed in a previous study [50].

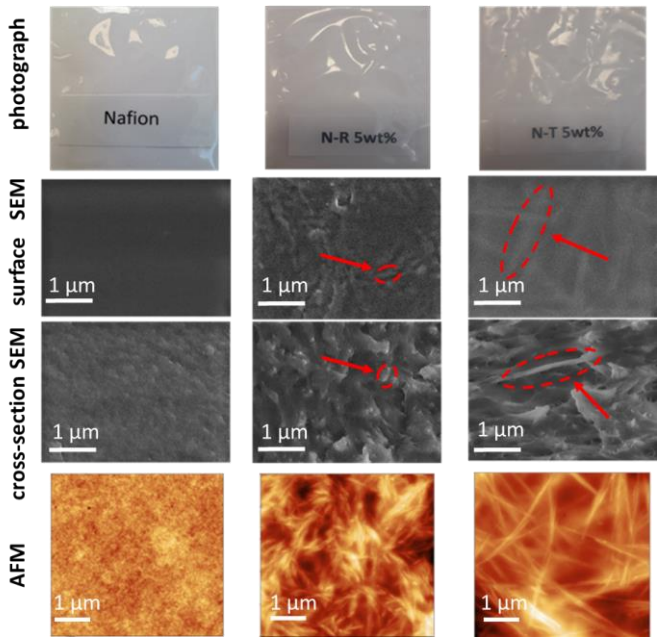

Figure 1. Photographs, SEM (surface and cross-section) and AFM topographic images of Nafion based membranes annealed at 100°C during 5 min: pure Nafion; N-R 5 wt. % and N-T 5 wt. %. Red arrows show some CNC rods in the Nafion matrix. For AFM images, the Z scale is [-2;2]nm for Nafion, [-50;50]nm for N-R 5 wt. % and [-80;80]nm for N-T 5wt. %.

Water uptake and swelling properties

The water uptake capacity, in-plane linear and thickness swellings of raw Nafion-CNC membranes with CNC contents varying from 0 to 10 wt. % are displayed in Fig. 2. The observed behaviors were similar for both N-R and N-T membranes. The water uptake (WU) increased first from 20 to 30 % for CNC content between 0 and 5 wt. % and then remained relatively constant at 30 % up to CNC 10 wt. %. Likewise, the thickness swelling ratio (TS) increased with the CNC content, going from 10 to 30 % when CNC content increased from 0 to 10 wt. %. Thus, WU and TS increases indicate the effective role of CNCs in keeping water molecules in the nanocomposite. In contrast, the in-plane linear swelling ratio (LS) decreased continuously from 10 to 4 %, particularly when the CNC content was greater than 5 wt. % whatever the origin of the CNC. This is in accordance with the existence of a critical percolation threshold of CNC in Nafion composite aided by matrix-CNC interactions, primarily by hydrogen bonds previously estimated at 5 wt. % [50], [57]. It is important to take this criterion into consideration in the context of the target application.

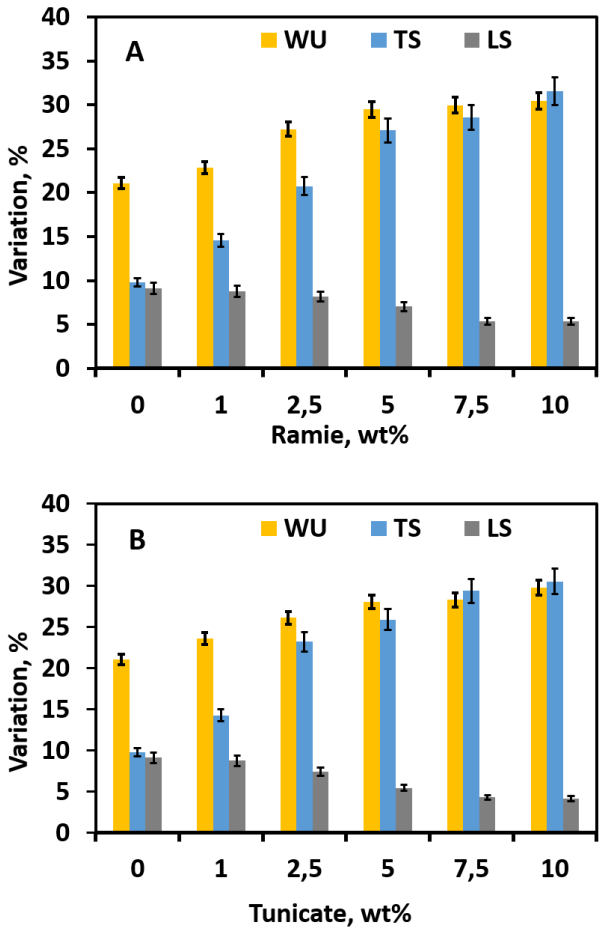

Figure 2: Swelling properties of Nafion membranes at various Ramie (A) and Tunicate (B) CNC contents. Water uptake (WU), thickness ratio (TS) and in-plane linear ratio (LS) were calculated using equations 2, 3 and 4.

Mechanical properties

Tensile properties, including strength, Young's modulus and elongation at break were determined on each membrane equilibrated at room temperature (Fig. 3). The stress-strain curves exhibited a bi-phasic behavior characterized by an initial linear stress-strain followed after yielding by a second horizontal phase until fracture for all N-R and N-T raw membranes annealed at 100°C during 5 min, as shown for N-R and N-T membranes containing 5 wt. % of CNC, (Fig. 3A). This bi-phasic behavior was widely observed in Nafion composites and in cellulose based composites [58]. Young's modulus calculated from the initial linear curve part increased from 0.2 to 0.5 and 1.0 GPa for N-R and N-T membranes respectively when CNC content increased from 0 to 10 wt. % (Fig. 3B). The tensile strength remained constant at 14 MPa for N-R membranes, but increased from 10 up to 29 MPa for N-T membranes in the same CNC content range (Fig. 3C). Finally, the mean values of the strain at break (values

between 10 and 150 %) tended to decrease with CNC wt. %, specifically for CNC contents greater than 5 wt. % (Fig. 3D). Beyond this CNC content, a strong decrease in the strain at break could be prejudicial for using such membranes for PEMFC applications. This CNC threshold value is related to the limit CNC content value of the percolation network phenomena obtained in similar dry composite membranes [57]. Moreover, the 4-fold higher aspect ratio value for Tunicate than for Ramie CNC (Table 1) can explain the 2-fold Young modulus enhancement with stable tensile strength and similar decrease in the strain at break. Nevertheless, mechanical softening will no doubt occur upon exposure to water on account of water diffusing into the matrix and competitively hydrogen bonding with the CNC surfaces which disrupts the stress-bearing CNC scaffold [57]. Moreover, the higher aspect ratio of Tunicate CNCs could explain the higher Young modulus and tensile strength values at break for raw membranes than those obtained with Ramie nanocrystals. Thus, in the following study, in view of these mechanical properties results combined to high water uptake and reasonable in-plane swelling and thickness swelling properties, the N-T 5 wt. % composite membrane was selected to study the effect of heat treatment on Nafion-CNC membrane performances in comparison with pure Nafion membrane.

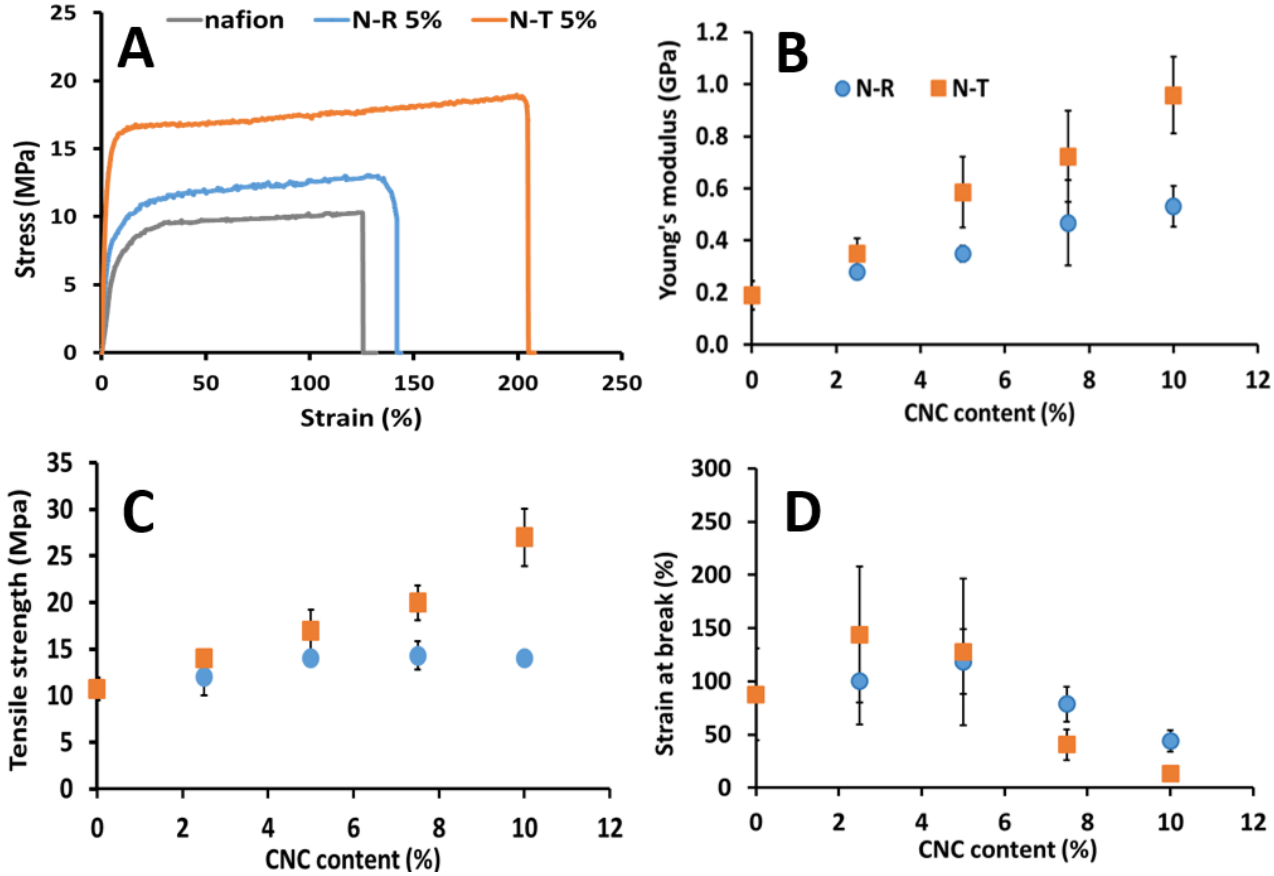

Figure 3: Mechanical properties of Nafion membranes at various Ramie and Tunicate CNC contents. All membranes were annealed at 100°C for 5min : (A) stress vs strain curves of pure Nafion, N-R 5 wt. % and N-T 5 wt. % membranes (B) Young's modulus, GPa.; (C) Tensile strength, MPa.; (D) Strain at break, %.

Thermal annealing effect on structural properties of Nafion-CNC membranes

Morphological characterizations

Raw Nafion and N-T 5 wt. % membranes were oven-annealed during 1h at different temperatures ranging from 100°C to 150°C. During thermal treatment, the N-T membranes became black when the annealing temperature was above 120°C, while Nafion membranes remained practically unchanged and transparent even after annealing at 150°C (Fig. 4). Note that similar behavior was also observed for N-R membranes (data not shown). The black coloration was already often observed when the acid hydrolysis of cellulose was performed in presence of a high concentration of sulfuric acid (pH < 1) at high temperature (T > 50°C). It reveals a partial degradation of cellulose chains with rupture of β-1-4 linkages between glucose molecule units without total dehydration of some of them. Total dehydration often occurs at temperatures above 467 °C or in a polar aprotic solvent [59, 60]. Moreover, the occurrence of chemical acid sulfate groups on Nafion and on CNC with a pKa value close to 1.9 can induce, in the vicinity of the sulfate groups, a decrease in the pH which could locally initiate a low degradation of arranged cellobiose chains on the surface of the rods.

Thermal properties

TGA experiments showed a weight loss in three approximatively stages for both Nafion and N-T 5 wt% membranes annealed up to 100°C or 150°C (SI-5 A and B). The first derivative traces (SI-5B) show the first loss less of 6 wt% from 30°C to 220°C, attributed undoubtedly to the loss of water and solvent traces in annealed membranes. Ir was also associated with the black coloring fot N-T membranes related to its surface degradation, favoring the implementation of specific interactions between Nafion and CNC surfaces. The second

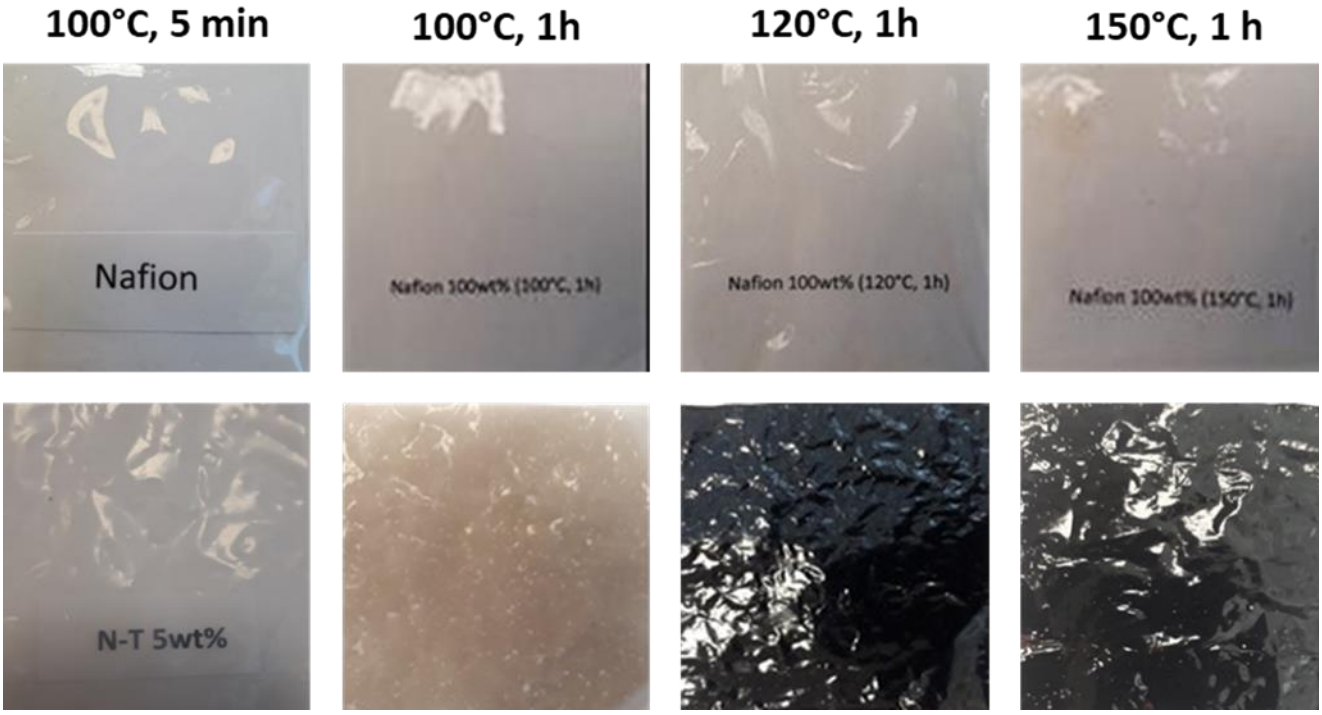

Figure 4: Photographs of Nafion and N-T 5 wt. % membranes annealed at 100 °C during 5 min and at different temperatures (100, 120 and 150°C) during 1 h and stabilized at ambient relative humidity.

Table 2 : Temperature changes for Tg, endothermic and exothermic peaks in Nafion and N-T 5 wt% annealed membranes

Membranes	Annealed temperature(°C)	Tg (°C)	$Peak_{exo}$(°C)	$Peak_{endo}$ I(°C)	Peak $_{endo}$II et III (°C)
Nafion	100	133.7	148.1	164.9	> 225
	150	157.2	-	193.0	> 225
N-T 5 wt%	100	not visible	180.0	198.3	> 200
	150	not visible	-	219.1	> 235

stage between 400 and 560 °C to the total decomposition of membranes as already observed by [61]. The presence of CNC dors not DSC curves (Figure SI-5 C and D) concern the first run at the heating rate of 10°C min^{-1}. Tg and temperature values of endothermic and exothermic peaks were described in Table 2 for both Nafion and N-T 5 wt% membranes annealed up to 100°C or 150°C. First, the Tg of Nafion membranes annealed respectively at 100°C and 150°C increases from 133.7 °C to 157.2 °C and can be due to the loss of water known to be act as a plasticizer. [61, 62] On the contrary, DSC curves of N-T membranes didn't show Tg and that can be explained by the And finally, first endothermic peak was observed at 164.9°C and 198.3°C for Nafion and N-T membranes annealed at 100°C, respectively. In accordance with another studies, it was assigned to the order-desorder molecular rearrangement transition which occurs inside the hydrophilic polar clusters of Nafion as a result of water present. [63, 64] The temperature increase of this endothermic transition (close to 30°C) tends to show that CNCs help to stabilize hydrophilic polar clusters. For membranes annealed at 150°C the first endothermic peak was detected at 193°C for N and 219.1°C for N-T. It could be also attributed to the order-desorder molecular rearrangement transition which occurs inside the hydrophilic polar clusters of Nafion but a contribution of the endothermic decomposition of acid –SO3H groups could not be ruled out. The following regions above 220°C would be related to the melting of hydrophobic part of Nafion polymer [61, 63]. change drastically the thermal properties of Nafion-based membranes after 220 °C.

decrease of Nafion chain mobility due to their strong interactions with CNC. Exothermic peaks were observed at 148.1 °C and 180°C for Nafion and N-T membranes annealed at 100°C, respectively and the peak for N membrane being much smaller than the one for N-T membrane. It can assigned by an increase of the crystalline phase of Nafion chains and especially in the vicinity of CNCs. After heat treatment at 150°C, this phenomena was not observed.

DSC curves after the second run adopt a flat shape which can suggest the degradation of membranes at 250°C as observed in figure SI-5 A and B.

Assessment of water accessibility of the dry membranes

The dry Nafion and N-T membranes were examined by dynamic vapor sorption measurements to investigate the state of water molecules in the dry microstructure network before analyzing their water swelling properties. The water sorption isotherms provide the numbers of water sorption sites (at low RH range) and of voids (at high RH range). These numbers depend on the cross-linkages implemented in the composite membrane. The water sorption isotherms of Nafion and N-T 5 wt. % membranes annealed between 100 and 150°C exhibited sigmoidal curves during water sorption and desorption in the 5-95% RH range (Fig. 5). When the thermal treatment was

carried out at 100°C or at 120 and 130°C (the same results were obtained for 120° C as for 130°C), the sorption-desorption curves of N-T membranes were slightly above those of Nafion membranes especially at high RH (from 50 to 95%). On the contrary, they were below those of pure Nafion membranes in the same RH range when annealed at 150°C. These differences did not exceed 2.5% of water content, at 95% RH, between the two membranes. With the high precision of the gravimetric analyzer's ultrasensitive microbalance used (0.1 mg), they were nevertheless significant.

To clarify these membrane behaviors, the water sorption isotherms were fitted by using the PARK model (Fig. 5). This analysis allowed us to distinguish three sorption mechanisms from the curves: between 0 and 20% RH, the formation of water sorption sites on the surface of the polymers (Nafion and CNCs), represented by the A_L parameters; between 20 and 60% RH, the linear sorption of water molecules following Henri's law (K_H parameter); and above 60% RH, the formation of water molecule aggregates represented by K_A and n [55].

The A_L, corresponding to the formation of a layer of water sorption sites on the polymer chains, varied between 0.06 and 0.010 g water/g of dry material for both raw and annealed membranes. The addition of CNC 5 wt. % did not show a clear increase in the water sorption sites at low RH values (Fig. 5, table). In the same manner, the K_H value, representing the formation of water molecule multilayers on polymer chains, tended to be the same from 100°C to 150°C for the Nafion and N-T membranes, between 0.09 and 0.11 g water/g dry matter, i.e. ten times more than water molecules adsorbed between 0 and 20 % RH. Larger variations were observed, however, at high RH values.

Differences between the Nafion and N-T membranes were clearly observed when the annealing temperature applied was below 150°C. K_a and n values increased up to 0.3 g water/g and 16.3 respectively for N-T membranes annealed at 120°C, whereas for Nafion membranes, these parameters remained around 0.19 g water/g and 9.5 (Fig. 5, table). At 150°C, K_a and n values decreased significantly 1-1.5 fold for both Nafion and N-T membranes and tended even to be similar (K_a = 0.12-0.13 g water/d and n = 9) for Nafion and N-T membranes.

These results indicate that the size and the number of the water molecule aggregates embedded in the Nafion membrane decreased strongly after the thermal treatment at 150°C, even in the presence of CNCs. Before this critical temperature value, the addition of CNC clearly induced an increase in the free volume in the composite network. Similarly, the hysteresis (%) exhibited between the sorption and desorption curves and calculated from the differences between water content values (C_D-C_S, %) was much less pronounced for annealed Nafion membranes than for annealed N-T membranes and for N-T membranes annealed at 150°C than for those annealed at 100°C (Fig. 5, insert). This demonstrates that the water retention was 3-fold higher for N-T annealed before 150°C than for pure Nafion membranes. Overall, the introduction of CNC in the Nafion matrix increased the number of OH sites in the membranes and favored the water uptake of the Nafion-based composite only when it was annealed at temperatures below 150°C (100 and 120°C). We also investigated the situation with regards to the water uptake and swelling properties after soaking (or total immersion) in deionized water.

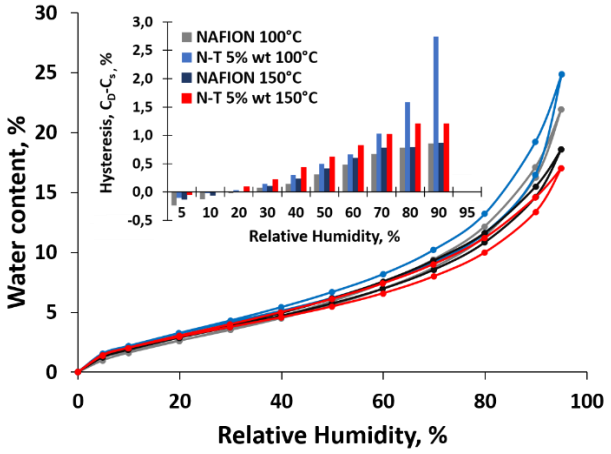

Nafion	$A_L \times 10^{-1}$	K_H	K_a	n	E
	$g_{water} \cdot g^{-1}_{dry\ matter}$				%
Raw	0.08	0.109	0.194	10.4	3
100°C	0.06	0.104	0.185	9.5	3.7
120°C	0.06	0.094	0.195	9.2	5.5
150°C	0.06	0.106	0.127	9.3	1.7

N-T 5 wt%	$A_L \times 10^{-1}$	K_H	K_a	n	E
	$g_{water} \cdot g^{-1}_{dry\ matter}$				%
Raw	0.10	0.104	0.189	10.9	2.2
100°C	0.09	0.114	0.277	14.7	4.0
120°C	0.06	0.112	0.299	16.3	7.5
150°C	0.10	0.091	0.116	9.2	2.0

Figure 5 : Water sorption isotherms and hysteresis (insert) of Nafion and N-T 5 wt. % raw and annealed membranes, at 100°C and 150°C, 1h. Tables : PARK parameters of Nafion and N-T 5 wt. % membranes; A_L, K_H, K_a (expressed in units of g water/g dry material) and n were calculated as in [48] between 5 and 95% RH corresponding to a water activity of 0.05 to 0.95. E, deviation modulus.

Water uptake and swelling properties of annealed membranes

The impact of heat treatment on the swelling properties of Nafion and N-T 5 w. % membranes was measured after water immersion for 72 hours at room temperature (Fig 6A). Nafion and N-T 5wt. % membranes annealed at 100°C during 5 min were taken as the reference.

For Nafion membranes, thermal annealing from 100 to 150 °C had no effect or only very slightly decreased the water uptake (WU from 21 to 18 %), the thickness swelling (TS from 10 to 8%) and the linear in-plane swelling parameter (LS 9-10 %), as shown in Fig 6A. The addition of 5 wt. % Tunicate led to a quite different situation: the WU and TS values of N-T membranes were 1.5 and 2.5 times higher than those of Nafion membranes (i.e. this has to be correlated to the 20% more bond water molecules in the composite at any annealing temperature). On the contrary, the LS parameters of N-T membranes were two times lower than those measured on Nafion membranes and remained stable at ~5% under thermal annealing. Thus, the presence of CNC promoted water uptake while the thickness of the membrane increased and its 2D plane dimensions decreased. Fig. 6B represents the volume increase (ΔV) as a function of water mass uptake (ΔM) for the different temperatures of the heat treatment. For the two systems (Nafion and N-T 5 wt. %) the relation between the ΔV and ΔM followed a distinct linear function (Fig. 6B). It shows that the water mass uptake was higher than the volume uptake of the corresponding mass uptake for N-T 5 wt. %.

The opposite situation was observed for Nafion where the volume increase was higher than the corresponding increase in the mass uptake. This is in agreement with the fact that water uptake is more constrained (especially in-plane) for N-T 5 wt.% than for Nafion and could be due to the presence of nanocrystals aligned parallel to the membrane surface, as observed on AFM topography images (Fig. 1).

Influence of the annealing processing on functional groups

In order to study the Nafion-CNC interactions at sub-molecular level, N-T 5 wt. % and pure Nafion membranes annealed in the 100-150°C temperature range were analyzed by ATR

spectroscopy and compared (Fig.7). FTIR spectra of the membranes were normalized and are presented from 4000 to 850 cm^{-1}.

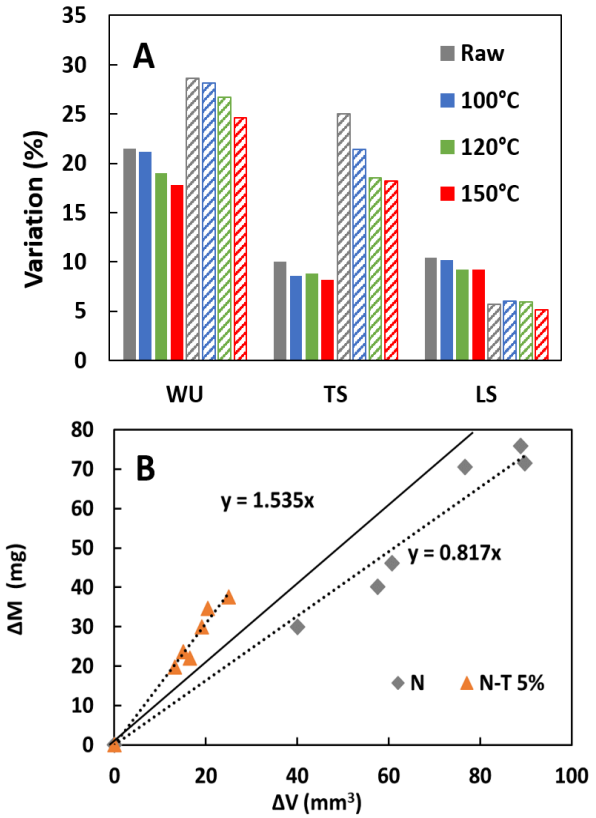

Figure 6: (A) Swelling properties (WU, TS and LS) and (B) relationship between the volume increase (ΔV) and the water mass uptake (ΔM) for Nafion (full) and N-T 5% wt (hatched) membranes annealed at different temperatures (100, 120 and 150°C) during 1 h. TS and LS were calculated according to equations 3 and 4. Raw sample was pure Nafion membrane annealed at 100 °C, 5 min., stabilized at ambient relative humidity.

For Nafion (Fig 7A), a broad band around 3500 cm^{-1} assigned to water molecules was observed. For N-T 5 wt. %, a broad intense spectral band assigned to the hydroxyl groups of Tunicate was observed between 3500 and 3250 cm^{-1} (Fig 7. B) that corresponds to the vibration of intramolecular and intermolecular OH bonded in CNC. Another band was observed between 2930 and 2850 cm^{-1} and corresponds to the asymmetric CH_2 vibration in cellulose from C6 (Fig. 7B) [65-68]. The intensities of all the bands in this region decreased with the increase in the annealing temperature of N-T 5 wt. % membranes from 100°C to 150°C. The spectra tended to be similar to those of the raw Nafion membrane above an annealing temperature of 120°C, indicating the decrease in the hydrogen bonds network in N-T 5 wt. % membrane above 120°C (Fig 7A and B). The increase of hydrogen bonds in N-T 5 wt. % membranes compared to Nafion and the decrease in hydrogen bonds with thermal annealing is in good agreement with the water sorption isotherms and swelling measurements of the membranes presented above with a WU higher for N-T 5 wt. % than for Nafion and a WU decrease with the thermal annealing temperature.

In the range 2000 - 1385 cm^{-1} (Fig 7C and D), Nafion spectra showed three characteristic bands: 1720 cm^{-1}, assigned to the asymmetric bending of the H_3O^+ counter ion of sulfate groups, 1628 cm^{-1} assigned to the bending frequency of water and 1438 cm^{-1} assigned to the vibrations of $–(S(O)_2 – O)–$ groups in Nafion (Fig 7C) [69, 70]. In presence of CNC, the band at 1720 cm^{-1} remained unmodified, the OH bending of water vibration was more pronounced at 1628 cm^{-1} as well as that of the $–(S(O)_2 – O)–$ groups between 1438 and 1428 cm^{-1} due to the presence of such groups in CNC (Fig 7D). The thermal annealing induced slight modifications in the Nafion spectra with a small decrease in the 1720 and 1438 cm^{-1} bands. For N-T 5 wt. %, thermal annealing induced in this case a strong decrease in the three bands in this region above 120°C. These decreases of the bands at 1720 and 1628 cm^{-1} with thermal annealing are again in good agreement with a WU decreasing with the thermal annealing temperature.

Finally, in the range 1350 – 850 cm^{-1} (Fig. 7E and F), apart from the bands coming from Nafion, characteristic absorption peaks [41, 42, 66-68, 71] were detected at 1034 cm^{-1} for

primary [41, 42, 71] and at 1055 cm^{-1} and 1120 cm^{-1} for secondary [66-68] alcohol groups of cellulose. The peak at 1034 cm^{-1} decreased progressively and then completely disappeared during membrane annealing from 100°C to 150°C. At the same time, the peak at 1055 cm^{-1} assigned to both the SO_3^- groups occurring in Nafion and the secondary alcohol of cellulose decreased partially (Fig. 7E and F) while the peaks at 1134, 1150 and 1197 cm^{-1} assigned respectively to $S(O)_2$ and $–(S(O)_2 – O)–$ stretching [72] increased until a perfect superposition of the spectrum with that of Nafion membrane annealed at 150°C was observed. The band at 1134 and 1150 cm^{-1} was especially well detected when the composite membrane was annealed at 130°C and 150°C. Thus, all these band changes could derive from the cross-linkage reactions between hydroxyl groups of cellulose and SO_3^- groups of cellulose and Nafion. Six reactions were considered: i- formation of an ether by condensation of two primary alcohols of cellulose (likely reaction); ii- sulfate ester formation by reaction of one alcohol function and a sulfate function, both coming from cellulose (likely reaction); iii- sulfonate ester formation by reaction of an alcohol function coming from cellulose and a sulfonic acid function coming from Nafion (likely reaction); iv- dehydration of two sulfate functions leading to a sulfate anhydride coming from cellulose (unlikely reaction); v- dehydration of one sulfate function and one sulfonic acid function leading to a sulfonate anhydride (unlikely reaction); and vi- dehydration of two sulfonic acid functions leading to a sulfonate anhydride, both coming from Nafion (likely reaction). These various reactions, detailed in the supporting information (SI 5), are not equivalent and do not exhibit the same thermal stability. A depletion in alcohol functions as shown by decrease in C-O alcohol bands at 1034 and 1055 cm^{-1}, a depletion in the sulfate function as shown by the evolution of the band at 1720 cm^{-1}, the formation of sulfate ester and anhydride, sulfonic ester and anhydride supported by the enhancement of the bands at 1120, 1134 and 1197 cm^{-1} attributed to SO_2 and SO_3 in such functionalities are coherent with ester formation and dehydration reactions, activated by thermal annealing above 130°C, the temperature at which the black color became increasingly intense (Fig. 4).

Influence of the annealing processing on mechanical properties

The mechanical properties of Nafion and N-T 5 wt. % annealed membranes were measured (Fig. 8). The impact of thermal annealing on the stress-strain curve was more complex in comparison with that measured on raw membranes (Fig. 3A). Overall, the stress-strain curves can be divided into 2 regions corresponding to the elastic (elongation from 0 to 2%) and plastic (elongation above 2%) regions (Fig. 8A). In the elastic region, the Young modulus of Nafion membranes remained constant at 0.2 ± 0.05 GPa (Fig. 8B) whatever the annealing temperature used, while after the addition of 5 wt. % CNC, it increased significantly from 0.6 ± 0.15 GPa to 1 ± 0.15 GPa when the annealing temperature increased from 100 to 120°C. Thereafter, it strongly decreased until 0.4 ± 0.1 GPa after thermal treatment of the N-T membrane above 130°C, i.e. a Young's modulus value twice as high as that of Nafion membrane. The tensile strength increased with the annealing temperature, from 10 to 15 MPa for pure Nafion and from 15 to 20 MPa for N-T 5 wt. % membranes (Fig. 8C). However, the strain at break values were lower for N-T membranes than those of Nafion membranes and did not exceed 75% for annealing temperatures between 100 and 130°C and was 125 % at 150°C. The strain at break of the Nafion membrane increased up to 250 % ± 50 % in the same thermal treatment range (Fig. 8D).

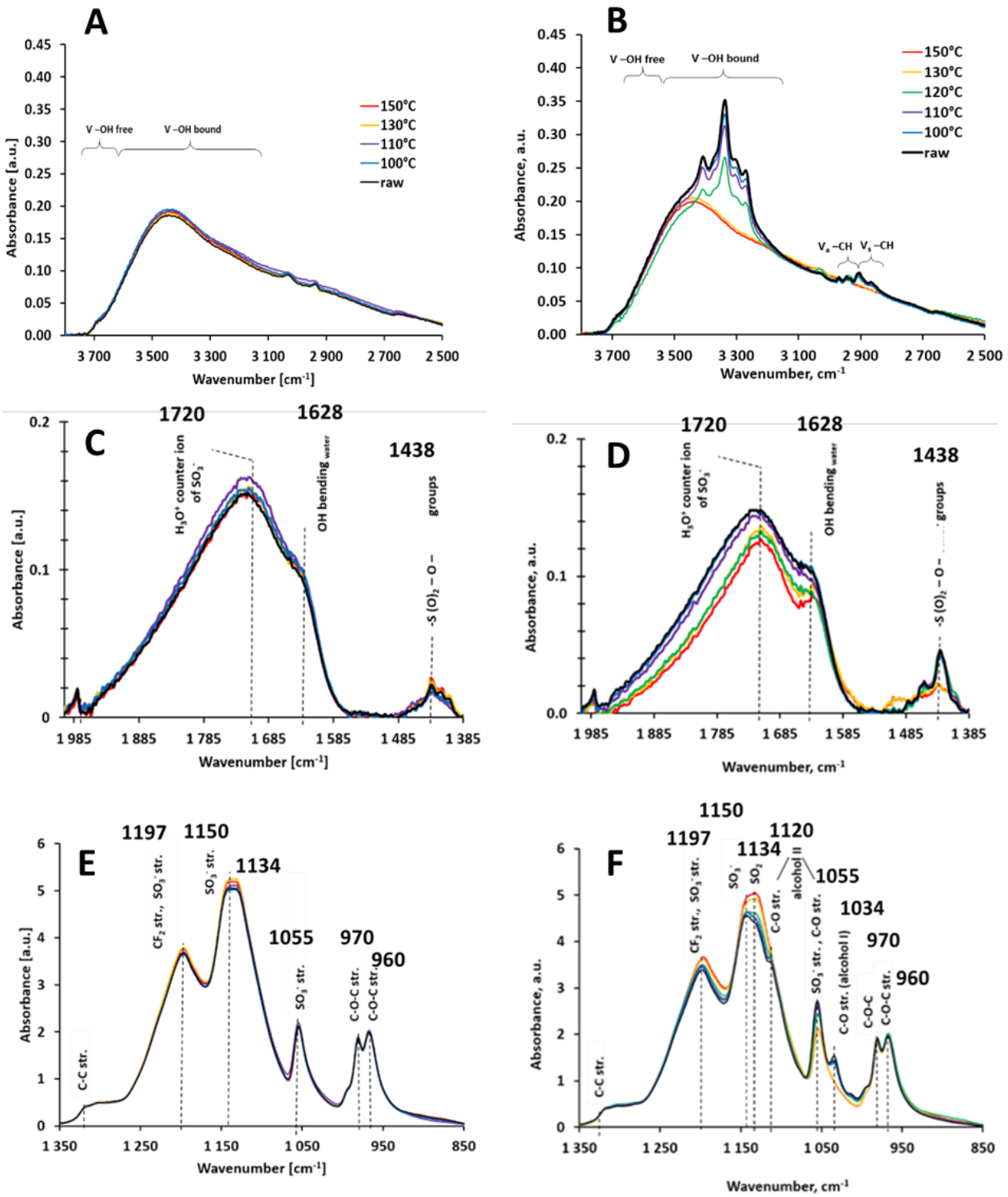

Figure 7 : FTIR spectra of pure Nafion (A,C,E) and N-T 5 wt. % (B,D,F) membranes annealed from 100 to 150°C, 1h. Raw membranes were annealed at 100 °C, 5 min.

Thus, the black color associated to the cross-linkage reactions demonstrated on N-T membranes treated beyond 120°C can explain the sudden decrease in the Young modulus and the increase in strain at break (%), and hence the lower in-plane swelling values shown in Fig. 6. On the contrary, the increase in both the Young modulus and tensile strength with the addition of CNC and annealing below 130°C could promote the ion exchange capacity and proton conductivity through the membrane which increased in thickness due to the water uptake (Fig. 6).

Impact on Ion exchange capacity (IEC), hydration number (λ) and proton conductivity properties

In order to investigate the proton exchange capacity of Nafion and N-T 5 wt. % membranes as a function of the thermal annealing conditions, the Ion Exchange Capacities (IEC) were measured and hydration numbers (λ) were determined (Fig. 9A and B).

Both raw membranes had similar IEC values 1.07 ± 0.01 meq.g^{-1} close to the one measured in previous studies [11]. The IEC value decreased from 1.07 to 1.04 meq.g^{-1} for Nafion and from 1.06 to 1.01 meq.g^{-1} for N-T 5 wt. % when the annealing temperature increased from 100°C to 150°C. The IEC decrease of Nafion membranes with annealing temperature may be the result of the weak formation of cross-linked network reflected in the FTIR spectra by only a slight reduction in the H_3O^+ counter ion of free SO_3^- sulfonic groups in Nafion at 1720 cm^{-1}, a system replaced by a few –(SO_2 – O) ether groups at 1438 cm^{-1} leading to the formation of anhydrides (Fig. 7B). In N-T 5 wt. % membrane, the reduction in the H_3O^+ counter ion of sulfonic groups at 1720 cm^{-1}, and the increase in –(SO_2 – O) ether groups at 1438 cm^{-1} as well as the increase in the OH bonding of water at 1628 cm^{-1} can explain the IEC differences of about 0.7 meq/g between Nafion and N-T 5 wt. % membranes. Nevertheless, when N-T membranes were annealed at 130°C and 150°C, the number of –(SO_2 – O) ether groups at 1438 cm^{-1} and OH water bonding observed at 1628 cm^{-1} decreased and could be associated with the decrease in the IEC. These cross-linkage reactions could contribute to a higher continuous decrease of IEC values for N-T membranes than for Nafion membranes (Fig. 9A and B). All these phenomena contribute to a greater reduction of SO_3^- groups in the N-T 5 wt. % compared to Nafion and thus a greater reduction in the proton exchange capacity of N-T 5 wt. % compared to Nafion.

The hydration number, λ, which reflects the number of water molecules per SO_3^- group, was calculated using Eq. 6 and is displayed in Fig. 9B. Like IEC, λ decreased with the annealing temperature from 13.5 to 9.5 and from 15.0 to 11.0 for Nafion and N-T 5 wt. % membranes, respectively. Contrary to IEC, the hydration number of Nafion was lower than that of the N-T 5 wt. % membranes. Although the sulfur content in Nafion membrane increased from 3.2 to 3.8 wt. % after adding CNC, the hydration number difference between the two is mostly related to the lower WU capacity of Nafion compared to N-T 5 wt. % membranes (Fig. 6A). The increased interaction between the hydrogen bonds and –(SO_2 – O) ether observed by FTIR (Fig. 7), as well as the occurrence of voids in the composite membrane identified by DVS measurements (Fig. 5), can explain this increase in hydration number at each annealing temperature, even above an annealing temperature of 150°C.

The proton conductivity, the significant property for fuel cell applications, was measured for Nafion and N-T 5 wt. % raw and annealed membranes from 100°C to 150°C (Fig 9C).

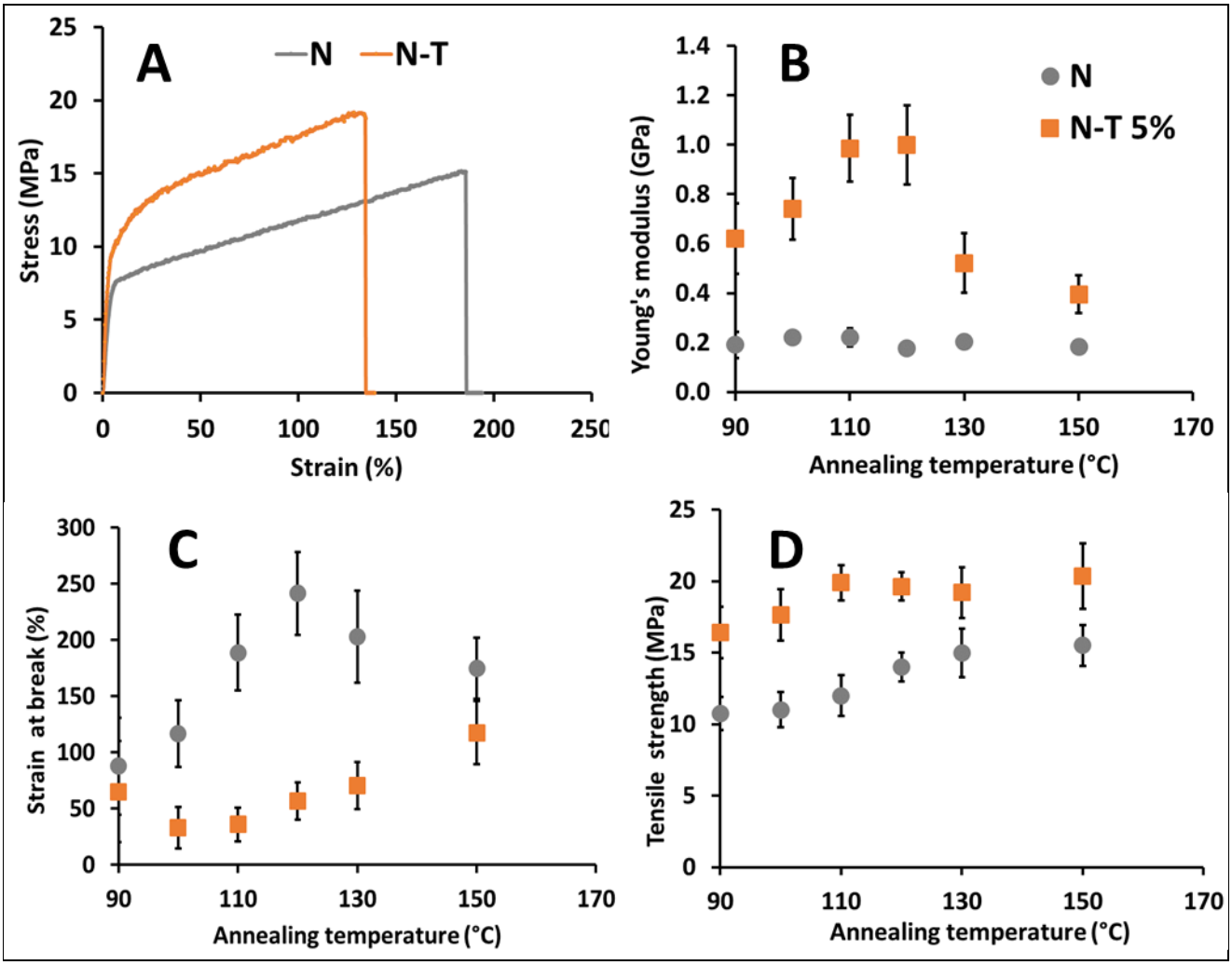

Figure 8: Mechanical properties of pure Nafion and N-T 5 wt. % membranes annealed from 100°C to 150°C, 1h; (A) stress vs strain curves; (B) Young's modulus in GPa ; (C) Tensile strength in MPa ; (D) Strain at break in %. Raw membranes were annealed at 100 °C, 5 min.

In the raw condition (5 min at 100°C), the presence of 5 wt. % of CNC in the Nafion membrane increased the conductivity slightly from 90 to 100 mS/cm thanks to a higher hydration number (Fig. 9B), no doubt thanks to a slight increase in sulfate groups (3.2 wt. % of sulfur for Nafion to 3.8 wt. % in N-T membranes, table 1).

Thermal annealing between 100°C and 130°C during 1 hour improved the proton conductivity of the Nafion membrane which rose to 110 mS/cm but it caused on the contrary a decrease in the proton conductivity of about 20 to 35% when CNCs were added, i.e. it fell to about 70 mS/cm. This decrease was linked to the IEC decrease and cross-linkage increase in the network, especially at high annealing temperature. Nevertheless, the proton conductivity value was preserved at 70 ± 5 mS/cm for N-T 5 wt. % membrane until the annealing temperature of 130°C and remains acceptable in fuel applications in comparison with another composite Nafion membrane such as Nafion/Laponite-p-styrene sulfonic acid [26](Fig. 9C).

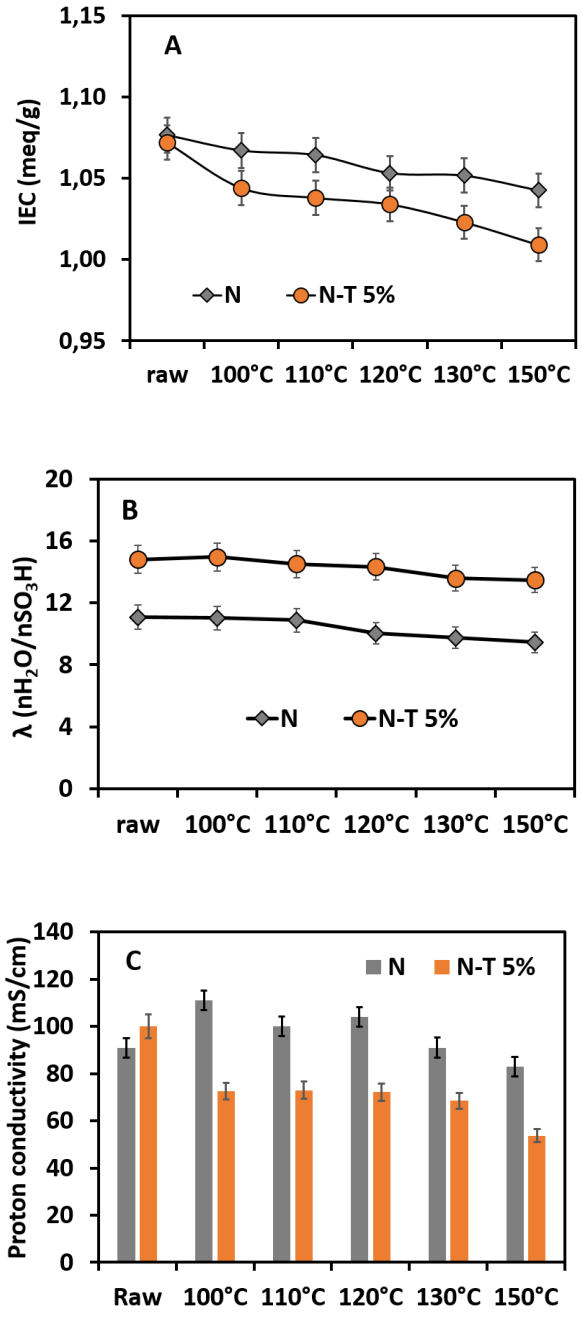

Figure 9: IEC (A), hydration number (B) and proton conductivity (C) of Nafion and N-T 5 wt. % membranes annealed from 100°C to 150°C during 1 hour and immersed in water during 24 hours. Raw samples were membranes annealed at 100 °C, 5 min

Conclusions

CNCs strongly modify the properties of Nafion membranes (Young's Modulus, dimensional stability, water uptake capacity...) and demonstrate their great interest as natural dopants for composite material preparation. Two series of membranes – Nafion with Ramie and Tunicate nanocrystals (CNCs with different lengths) – were prepared and annealed 5 min at 100°C in order to examine the influence of the size of the cellulose nanocrystals on the properties of the composite membranes. Digital, AFM and SEM Microscopies showed an excellent dispersion of the cellulose nanocrystals in the Nafion polymer. The water uptake capacity increased with the amount of CNCs in the composite membranes for both Ramie and Tunicate nanocrystals. At the same time, membrane surface area swelling decreased and thickness swelling increased with the amount of CNCs in composite membranes. These parameters are mandatory for proton exchange membrane fuel cell applications. It was shown that the Young modulus increased with the amount of CNCs in these membranes, regardless of the type of nanocrystals used (Ramie or Tunicate). These changes were stronger for Nafion-Tunicate membranes (needle-like nanocrystals measuring 2000 nm in length) than for Nafion-Ramie membranes. The Nafion-Tunicate N-T 5 wt. % composite membrane was thus selected to study the effect of heat treatment on membrane performances in comparison with pure Nafion membrane in the temperature range between 100°C and 150°C. The state of water molecules in the dry microstructure network was analyzed using dynamic vapor sorption measurements. Below 60 % RH, the behavior of the N-T 5 wt. % membrane was quite similar to that of the pure Nafion membrane. Above 60 % RH, differences

between Nafion and N-T membranes were clearly observed: the size and the number of water molecule aggregates (or clusters) embedded in the membrane were greater in N-T than in Nafion membranes but decreased strongly after the thermal treatment at 150°C, even in the presence of CNCs. This is coherent with the higher water uptake of N-T 5 wt. % than of Nafion and which decreases with the thermal annealing temperature. The dimensional stability of N-T 5 wt. % (especially the in-plane linear swelling) was better that that of pure Nafion membrane.

During the annealing process, Nafion and N-T 5 wt. % membranes lost less than 5% of weight when heated up to 150°C. The N-T 5 wt. % membrane became black, while the Nafion membrane remained unchanged and transparent after annealing at 150°C. Using FTIR, it was demonstrated that in Nafion membranes thermal annealing has little impact. In presence of CNCs, thermal annealing up to 130°C induced a loss of hydroxyl groups of cellulose but also induced crosslinking reactions leading to the formation of ether, ester and anhydride groups which could be correlated to the black color, the exothermic peak assigned by an increase of ordered Nafion chains in the vicinity of CNCs and the increase in the Young modulus of the membranes. The decrease in the Young modulus and strain at break of the composite membranes above 130°C could be correlated to the decomposition of some of the above-mentioned groups. The ion exchange capacity and hydration number of both pure Nafion and N-T 5 wt. % membranes decreased slightly with annealing temperature, indicating the existence of reactions of proton exchange groups (sulfate groups) under thermal annealing, which were even more pronounced in the presence of cellulose nanocrystals.

From the results presented above, we can conclude that the design of Nafion-CNC composite membranes is a very promising way in fuel cell field because first, CNCs increase water uptake while decreasing in-plane swelling. Secondly, CNCs increase membrane stiffness and thermal stability as is required for fuel cell applications in total hydrated medium. They could also decrease hydrogen permeation by increasing tortuosity inside the membranes. Then, hydrogen permeation and PEMFC performance measurements will be planned in a future study.

Acknowledgements

This research was supported by Region Centre Val de Loire, France, as part of the ARD2020 LAVOISIER program through the UMANITHY project. Fréderic Mahut and Raphael Coste are thanked for AFM characterizations.

Declarations

Conflict of interests. The authors declare that they have no conflict of interest.

References

[1] Bose S, Kuila T, Thi XLN, Kim NH, Lau KT, Lee JH. Polymer membranes for high temperature proton exchange membrane fuel cell: Recent advances and challenges. Progress in Polymer Science. 2011;36:813-43.

[2] Wang Y, Chen KS, Mishler J, Cho SC, Adroher XC. A review of polymer electrolyte membrane fuel cells: Technology, applications, and needs on fundamental research. Applied Energy. 2011;88:981-1007.

[3] Kim DJ, Jo MJ, Nam SY. A review of polymer-nanocomposite electrolyte membranes for fuel cell application. Journal of Industrial and Engineering Chemistry. 2015;21:36-52.

[4] Sapkota P, Boyer C, Dutta R, Cazorla C, Aguey-Zinsou KF. Planar polymer electrolyte membrane fuel cells: powering portable devices from hydrogen. Sustainable Energy & Fuels. 2020;4:439-68.

[5] Alaswad A, Omran A, Sodre JR, Wilberforce T, Pignatelli G, Dassisti M, et al. Technical and Commercial Challenges of Proton-Exchange Membrane (PEM) Fuel Cells. Energies. 2021;14. https://doi.org/10.3390/en14010144

[6] Walkowiak-Kulikowska J, Wolska J, Koroniak H. Polymers application in proton exchange membranes for fuel cells (PEMFCs). Physical Sciences Reviews. 2017;2. https://doi.org/10.1515/psr-2017-0018

[7] Hsu WY, Gierke TD. Ion-Transport and Clustering in Nafion Perfluorinated Membranes. Journal of Membrane Science. 1983;13:307-26.

[8] Rubatat L, Gebel G, Diat O. Fibrillar structure of Nafion: Matching Fourier and real space studies of corresponding films and solutions. Macromolecules. 2004;37:7772-83.

[9] Bakangura E, Wu L, Ge L, Yang ZJ, Xu TW. Mixed matrix proton exchange membranes for fuel cells: State of the art and perspectives. Progress in Polymer Science. 2016;57:103-52.

[10] Karimi MB, Mohammadi F, Hooshyari K. Recent approaches to improve Nafion performance for fuel cell applications: A review. International Journal of Hydrogen Energy. 2019;44:28919-38.

[11] Tritt-Goc J, Lindner L, Bielejewski M, Markiewicz E, Pankiewicz R. Synthesis, thermal properties, conductivity and lifetime of proton conductors based on nanocrystalline cellulose surface-functionalized with triazole and imidazole. International Journal of Hydrogen Energy. 2020;45:13365-75.

[12] Choudhury RR, Sahoo SK, Gohil JM. Potential of bioinspired cellulose nanomaterials and nanocomposite membranes thereof for water treatment and fuel cell applications. Cellulose. 2020;27:6719-46.

[13] Borup R, Meyers J, Pivovar B, Kim YS, Mukundan R, Garland N, et al. Scientific aspects of polymer electrolyte fuel cell durability and degradation. Chemical Reviews. 2007;107:3904-51.

[14] Dickinson EJF, Smith G. Modelling the Proton-Conductive Membrane in Practical Polymer Electrolyte Membrane Fuel Cell (PEMFC) Simulation: A Review. Membranes. 2020;10.

[15] Safronova E, Golubenko D, Pourcelly G, Yaroslavtsev A. Mechanical properties and influence of straining on ion conductivity of perfluorosulfonic acid Nafion (R)-type membranes depending on water uptake. Journal of Membrane Science. 2015;473:218-25.

[16] Shi SW, Chen G, Wang ZF, Chen X. Mechanical properties of Nafion 212 proton exchange membrane subjected to hygrothermal aging. Journal of Power Sources. 2013;238:318-23.

[17] Theiler A, Karpenko-Jereb L. Modelling of the mechanical durability of constrained Nafion membrane under humidity cycling. International Journal of Hydrogen Energy. 2015;40:9773-82.

[18] Xiao P, Li JS, Tang HL, Wang Z, Pan M. Physically stable and high performance Aquivion/ePTFE composite membrane for high temperature fuel cell application. Journal of Membrane Science. 2013;442:65-71.

[19] Amjadi M, Rowshanzamir S, Peighambardoust SJ, Sedghi S. Preparation, characterization and cell performance of durable nafion/SiO2 hybrid membrane for high-temperature polymeric fuel cells. Journal of Power Sources. 2012;210:350-7.

[20] Dresch MA, Isidoro RA, Linardi M, Rey JFQ, Fonseca FC, Santiago EI. Influence of sol-gel media on the properties of Nafion-SiO2 hybrid electrolytes for high performance proton exchange membrane fuel cells operating at high temperature and low humidity. Electrochimica Acta. 2013;94:353-9.

[21] Gerasimova E, Safronova E, Ukshe A, Dobrovolsky Y, Yaroslavtsev A. Electrocatalytic and transport properties of hybrid Nafion (R) membranes doped with silica and cesium acid salt of phosphotungstic acid in hydrogen fuel cells. Chemical Engineering Journal. 2016;305:121-8.

[22] Tang HL, Pan M. Synthesis and characterization of a self-assembled nafion/silica nanocomposite membrane for polymer electrolyte membrane fuel cells. Journal of Physical Chemistry C. 2008;112:11556-68.

[23] Tang HL, Wan Z, Pan M, Jiang SP. Self-assembled Nafion-silica nanoparticles for elevated-high temperature polymer electrolyte membrane fuel cells. Electrochemistry Communications. 2007;9:2003-8.
[24] Santiago EI, Isidoro RA, Dresch MA, Matos BR, Linardi M, Fonseca FC. Nafion-TiO2 hybrid electrolytes for stable operation of PEM fuel cells at high temperature. Electrochimica Acta. 2009;54:4111-7.
[25] Taghizadeh MT, Vatanparast M. Ultrasonic-assisted synthesis of ZrO2 nanoparticles and their application to improve the chemical stability of Nafion membrane in proton exchange membrane (PEM) fuel cells. Journal of Colloid and Interface Science. 2016;483:1-10.
[26] Fatyeyeva K, Bigarre J, Blondel B, Galiano H, Gaud D, Lecardeur M, et al. Grafting of p-styrene sulfonate and 1,3-propane sultone onto Laponite for proton exchange membrane fuel cell application. Journal of Membrane Science. 2011;366:33-42.
[27] Zhang B, Cao Y, Jiang ST, Li Z, He GW, Wu H. Enhanced proton conductivity of Nafion nanohybrid membrane incorporated with phosphonic acid functionalized graphene oxide at elevated temperature and low humidity. Journal of Membrane Science. 2016;518:243-53.
[28] Yin CS, Xiong BY, Liu QC, Li JJ, Qian LB, Zhou YW, et al. Lateral-aligned sulfonated carbon-nanotubes/Nafion composite membranes with high proton conductivity and improved mechanical properties. Journal of Membrane Science. 2019;591.
[29] Teixeira FC, de Sa AI, Teixeira APS, Rangel CM. Nafion phosphonic acid composite membranes for proton exchange membranes fuel cells. Applied Surface Science. 2019;487:889-97.
[30] Tsai JC, Lin CK. Effect of PTFE content in gas diffusion layer based on Nafion (R)/PTFE membrane for low humidity proton exchange membrane fuel cell. Journal of the Taiwan Institute of Chemical Engineers. 2011;42:945-51.
[31] Albu AM, Maior I, Nicolae CA, Bocaneala FL. Novel Pva Proton Conducting Membranes Doped with Polyaniline Generated by in-Situ Polymerization. Electrochimica Acta. 2016;211:911-7.
[32] Malinowski M, Iwan A, Parafiniuk K, Gorecki L, Pasciak G. Electrochemical properties of PEM fuel cells based on Nafion-polybenzimidazole-imidazole hybrid membranes. International Journal of Hydrogen Energy. 2015;40:833-40.
[33] Molla S, Compan V. Performance of composite Nafion/PVA membranes for direct methanol fuel cells. Journal of Power Sources. 2011;196:2699-708.
[34] Park HS, Kim YJ, Hong WH, Lee HK. Physical and electrochemical properties of Nafion/polypyrrole composite membrane for DMFC. Journal of Membrane Science. 2006;272:28-36.
[35] Yao J, Xu GX, Zhao ZM, Guo J, Li SH, Cai WW, et al. An enhanced proton conductivity and reduced methanol permeability composite membrane prepared by sulfonated covalent organic nanosheets/Nafion. International Journal of Hydrogen Energy. 2019;44:24985-96.
[36] Ru CY, Gu YY, Duan YT, Na H, Zhao CJ. Nafion based semi-interpenetrating polymer network membranes from a cross-linkable SPAEK and a fluorinated epoxy resin for DMFCs. Electrochimica Acta. 2019;324.
[37] Eichhorn SJ, Dufresne A, Aranguren M, Marcovich NE, Capadona JR, Rowan SJ, et al. Review: current international research into cellulose nanofibres and nanocomposites. Journal of Materials Science. 2010;45:1-33. https://doi.org/10.1007/s10853-009-3874-0
[38] Eichhorn SJ, Gandini A. Materials from Renewable Resources. Mrs Bulletin. 2010;35:187-90.
[39] Klemm D, Kramer F, Moritz S, Lindstrom T, Ankerfors M, Gray D, et al. Nanocelluloses: A New Family of Nature-Based Materials. Angewandte Chemie-International Edition. 2011;50:5438-66.
[40] Dufresne A. Nanocellulose: a new ageless bionanomaterial. Materials Today. 2013;16:220-7.
[41] Hambardzumyan A, Foulon L, Bercu NB, Pernes M, Maigret JE, Molinari M, et al. Organosolv lignin as natural grafting additive to improve the water resistance of films using cellulose nanocrystals. Chemical Engineering Journal. 2015;264:780-8.
[42] Hambardzumyan A, Foulon L, Chabbert B, Aguie-Beghin V. Natural Organic UV-Absorbent Coatings Based on Cellulose and Lignin: Designed Effects on Spectroscopic Properties. Biomacromolecules. 2012;13:4081-8.
[43] Aguié-Béghin V, Païs G, Molinari M, Chabbert B. Films and Coatings from Lignocellulosic Polymers. Edible Films and Coatings: Fundamentals and Applications: CRC Press Taylor&Francis Group; 2017. p. pp 598.
[44] Lasrado D, Ahankari S, Kar K. Nanocellulose-based polymer composites for energy applications-A review. Journal of Applied Polymer Science. 2020;137. https://doi.org/10.1002/app.4895D
[45] Da Silva Perez D, Ruggiero R, Morais LC, Machado AEH, Mazeau K. Theoretical and experimental studies on the adsorption of aromatic compounds onto cellulose. Langmuir. 2004;20:3151-8.
[46] Chen X, Yuan FS, Zhang H, Huang Y, Yang JZ, Sun DP. Recent approaches and future prospects of bacterial cellulose-based electroconductive materials. Journal of Materials Science. 2016;51:5573-88. https://doi.org/10.1007/s10853-016-9899-2
[47] Noonan C, Tajvidi M, Tayeb AH, Shahinpoor M, Tabatabaie SE. Structure-Property Relationships in Hybrid Cellulose Nanofibrils/Nafion-Based Ionic

Polymer-Metal Composites. Materials. 2019;12. https://doi.org/10.3390/ma12081269
[48] Wang LK, Zuo XH, Raut A, Isseroff R, Xue Y, Zhou YC, et al. Operation of proton exchange membrane (PEM) fuel cells using natural cellulose fiber membranes. Sustainable Energy & Fuels. 2019;3:2725-32.
[49] Sriruangrungkamol A, Chonkaew W. Modification of nanocellulose membrane by impregnation method with sulfosuccinic acid for direct methanol fuel cell applications. Polymer Bulletin. https://doi.org/10.1007/s00289-020-03289-y
[50] Hasani-Sadrabadi MM, Dashtimoghadam E, Nasseri R, Karkhaneh A, Majedi FS, Mokarram N, et al. Cellulose nanowhiskers to regulate the microstructure of perfluorosulfonate ionomers for high-performance fuel cells. Journal of Materials Chemistry A. 2014;2:11334-40.
[51] Jiang GP, Zhang J, Qiao JL, Jiang YM, Zarrin H, Chen ZW, et al. Bacterial nanocellulose/Nafion composite membranes for low temperature polymer electrolyte fuel cells. Journal of Power Sources. 2015;273:697-706.
[52] Aguié-Béghin V, Molinari M, Hambardzumyan A, Foulon L, Habibi Y, T. H, et al. Preparation of ordered films from cellulose nanocrystals. . In: Roman eM, editor. Model Cellulosic Surfaces. ACS Symposium Series Book, ACS Division of Cellulose and Renewable Material ed: ACS; 2009. p. pp 115-36.
[53] Marcuello C, Foulon L, Chabbert B, Molinari M, Aguie-Beghin V. Langmuir-Blodgett Procedure to Precisely Control the Coverage of Functionalized AFM Cantilevers for SMFS Measurements: Application with Cellulose Nanocrystals. Langmuir. 2018;34:9376-86.
[54] Iwamoto S, Kai WH, Isogai A, Iwata T. Elastic Modulus of Single Cellulose Microfibrils from Tunicate Measured by Atomic Force Microscopy. Biomacromolecules. 2009;10:2571-6.
[55] Muraille L, Aguie-Beghin V, Chabbert B, Molinari M. Bioinspired lignocellulosic films to understand the mechanical properties of lignified plant cell walls at nanoscale. Scientific Reports. 2017;7. https://doi.org/10.1038/srep44065
[56] Lahiji RR, Xu X, Reifenberger R, Raman A, Rudie A, Moon RJ. Atomic Force Microscopy Characterization of Cellulose Nanocrystals. Langmuir. 2010;26:4480-8.
[57] Fox JD, Capadona JR, Marasco PD, Rowan SJ. Bioinspired Water-Enhanced Mechanical Gradient Nanocomposite Films That Mimic the Architecture and Properties of the Squid Beak. Journal of the American Chemical Society. 2013;135:5167-74.
[58] Gindl W, Keckes J. Tensile properties of cellulose acetate butyrate composites reinforced with bacterial cellulose. Composites Science and Technology. 2004;64:2407-13.
[59] Cao F, Schwartz TJ, McClelland DJ, Krishna SH, Dumesic JA, Huber GW. Dehydration of cellulose to levoglucosenone using polar aprotic solvents. Energy & Environmental Science. 2015;8:1808-15.
[60] Zhu C, Krumm C, Facas GG, Neurock M, Dauenhauer PJ. Energetics of cellulose and cyclodextrin glycosidic bond cleavage. Reaction Chemistry & Engineering. 2017;2:201-14.
[61] de Almeida SH, Kawano Y. Thermal behavior of Nafion membranes. Journal of Thermal Analysis and Calorimetry. 1999;58:569-77.
[62] Jung H-Y, Won Kim J. Role of the glass transtion temperature of Nafion 117 membrane in the preparation of the mebrane electrode assembly in a direct methanol fuel cell (DMFC). International Journal of hydrogen energy. 2012;37:12580-5.
[63] Lin H-L, Yu TL, Huang C-H, Lin T-L. Morphology study of Nafion membranes prepared by solutions casting. Journal of Polymer Science Part B-Polymer Physics. 2005;43:3044-57.
[64] Molla S, Compan V. Polyvinyl alcohol nanofiber reinforced Nafion membranes for fuel cell applications. Journal of Membrane Science. 2011;372:191-200.
[65] Schwanninger M, Rodrigues JC, Pereira H, Hinterstoisser B. Effects of short-time vibratory ball milling on the shape of FT-IR spectra of wood and cellulose. Vibrational Spectroscopy. 2004;36:23-40.
[66] Abidi N, Cabrales L, Haigler CH. Changes in the cell wall and cellulose content of developing cotton fibers investigated by FTIR spectroscopy. Carbohydrate Polymers. 2014;100:9-16.
[67] Grube M, Shvirksts K, Denina I, Ruklisa M, Semjonovs P. Fourier-transform infrared spectroscopic analyses of cellulose from different bacterial cultivations using microspectroscopy and a high-throughput screening device. Vibrational Spectroscopy. 2016;84:53-7.
[68] Kacurakova M, Smith AC, Gidley MJ, Wilson RH. Molecular interactions in bacterial cellulose composites studied by 1D FT-IR and dynamic 2D FT-IR spectroscopy. Carbohydrate Research. 2002;337:1145-53.
[69] Alentiev A, Kostina J, Bondarenko G. Chemical aging of Nafion: FTIR study. Desalination. 2006;200:32-3.
[70] Collette FM, Lorentz C, Gebel G, Thominette F. Hygrothermal aging of Nafion (R). Journal of Membrane Science. 2009;330:21-9.
[71] Samir M, Alloin F, Dufresne A. Review of recent research into cellulosic whiskers, their properties and their application in nanocomposite field. Biomacromolecules. 2005;6:612-26.
[72] Gruger A, Regis A, Schmatko T, Colomban P. Nanostructure of Nafion (R) membranes at different states of hydration - An IR and Raman study. Vibrational Spectroscopy. 2001;26:215-25.